



Available online at www.sciencedirect.com



Reliability Engineering and System Safety 00 (2014) 1–20

Reliability
Engineer-
ing &
System
Safety

Coupling mode-destination accessibility with a quantitative seismic-risk assessment to identify at-risk communities

Mahalia Miller^a, Jack W. Baker^a

^a*Stanford University, Stanford, CA USA*

Abstract

In this paper, we develop a framework for coupling mode-destination accessibility with a quantitative seismic-risk assessment to identify communities at a high risk for travel disruptions after an earthquake. For a case study of the San Francisco Bay Area, we find that accessibility varies more strongly from location to location than between income classes, and we identify particularly at-risk communities. We also observe that communities more conducive to local trips by foot or bike are predicted to be less impacted by losses in accessibility.

© 2014 Published by Elsevier Ltd.

Keywords: Infrastructure, Risk, Earthquakes

1. Introduction

Seismic risk assessment in earthquake engineering tends to focus on buildings, bridges, and the performance of infrastructure systems. For measuring the performance of transportation systems, researchers typically use engineering-based metrics such as the post-earthquake connectivity loss, which quantifies the decrease in the number of origins or generators connected to a destination node [e.g., 1], or the post-earthquake travel distance between two locations of interest [e.g., 2]. These frameworks have provided insight into seismic vulnerability and possible risk mitigation. However, the link to the human ramifications can be limited.

In the field of vulnerability sciences, researchers have long stressed the importance of the impact on human welfare from earthquakes. For example, Bolin and Stanford write that, “‘Natural’ disasters have more to do with the social, political, and economic aspects than they do with the environmental hazards that trigger them. Disasters occur at the interface of vulnerable people and hazardous environments” [3]. A recent World Bank and United Nations report echoed this idea that the effects on human welfare turn natural hazards into disasters [4].

Historical events emphasize the complex social effects of earthquakes. For example, on one hand the 1994 Northridge earthquake caused major damage to nine bridges, which, while significant, represented only 0.5% of the bridges estimated by Caltrans to have experienced significant shaking [5]. On the other hand, over half of businesses reported closing after the earthquake with 56% citing the “inability of employees to get to work” as a reason [6]. Furthermore, the total economic cost of transport-related interruptions (“commuting, inhibited customer access, and shipping and supply disruptions”) from this earthquake is estimated at 2.16 billion USD (2014) [7], using the consumer price index to account for inflation.

An emergent trend in earthquake engineering related to the social impacts is measuring the cumulative extra time needed for travel after an earthquake, sometimes called travel time delay [e.g., 8, 9]. This performance measure captures basic re-routing due to road closures and enables identifying roads more likely to be very congested. Travel time

23 approximately measures one aspect of impact on people, but does not capture the fact that some destinations and trips
 24 have higher value than others. Furthermore, this approach measures the impacts by focusing on aggregate regional
 25 effects rather than individual communities and demographic groups. Some recent work has looked at other metrics,
 26 such as the qualitative criteria-based metric “disruption index” [10]. However, this does not provide a quantitative link
 27 between the technical impact and the human ramifications. Other work has looked at resiliency, but defined it in pure
 28 engineering terms, such as percentage of a simplified road network that is functional [11]. Outside of transportation
 29 systems, some researchers have investigated the interplay between earthquake damage, such as damage to the electric
 30 power and wastewater networks, and the usability of houses and other buildings; this represents an important first
 31 step [12].

32 In contrast to the work on transportation-related seismic risk, urban planning has a long tradition of studying the
 33 impact on people of events and policy [13]. Accessibility is one metric popular in urban planning to measure
 34 the impact of different transportation network scenarios, and it measures how easily people can get to desirable
 35 destinations, which is one measure of social impact [14]. Furthermore, accessibility, by definition, quantifies one
 36 key aspect of human welfare [e.g., 14]. Within urban planning, accessibility has been measured in many ways,
 37 including individual accessibility, economic benefits of accessibility, and mode-destination accessibility [15]. The
 38 mode-destination accessibility is computed by taking the log value of the sum of a function of the utilities of each
 39 destination over all possible destinations and travel modes, where the utility decreases if getting to that destination is
 40 more costly or time-intensive [16]. This choice of accessibility definition is particularly applicable to quantifying the
 41 impacts of catastrophes, such as earthquakes, because certain destinations might be more critical for people in certain
 42 locations or from different socio-economic groups (such as low income or high income). However, this accessibility
 43 measure has not yet been linked to risk assessment. In addition, the majority of work to date assumes that travel
 44 demand and mode choice will remain unchanged after a future earthquake, which historical data suggests is not the
 45 case [7]. A first step towards considering variable demand is work in the literature that varies demand by applying a
 46 constant multiplicative factor on all pre-earthquake travel demand [8].

47 In this paper, we develop a framework for coupling mode-destination accessibility with a quantitative seismic-risk
 48 assessment to identify at-risk populations and measure the accompanying impacts on human welfare. We illustrate our
 49 approach with a case study of the San Francisco Bay Area transportation network, including highways, local roads,
 50 and public transportation lines. This study analyzes a set of forty hazard-consistent earthquake scenarios, ground-
 51 motion intensity maps, and damage maps, as we introduced in [17] using the optimization procedure we proposed
 52 in [18]. For each of these damage maps, we model damage with a practical, agent-based transportation model used by
 53 the local transportation authorities that includes damage to bridges, roads, and transit lines, and varies demand. Then,
 54 with this model, we estimate the predicted losses in accessibility according to 12 socio-economic groups used by local
 55 planners for the case study region, based on income class, and ratio of personal vehicles to workers in a household.

56 2. Case study: San Francisco Bay Area

57 2.1. Case study overview

58 We focus on the San Francisco Bay Area, a seismically-active region, to illustrate our approach (Figure 1). The
 59 area follows a polycentric metropolitan form, with San Francisco as the primary center and other jobs concentrated
 60 in suburban centers, such as Silicon Valley [19]. The region has a wide array of trip patterns for mandatory and
 61 non-mandatory trips. Furthermore, trip times and routes vary greatly depending on travel preferences and workplace
 62 locations [19]. Thus, we might expect noticeable disparities between households in the risk of travel time delays due
 63 to earthquakes.

64 This analysis considers the complex web of roads and transit networks of the case study area. The roads are
 65 modeled by a directed graph $G = (V, E)$, where V is a finite set of vertices representing intersections, and the set E ,
 66 whose elements are edges representing road links, is a binary relation on V . In this model, $(|V|, |E|) = (11,921, 32,858)$
 67 including centroidal links and $(|V|, |E|) = (9,635, 24,404)$ without. Centroidal links do not correspond to particular
 68 physical roads but instead capture more subtle travel flows, such as from outside the study area or the flow of people
 69 to and from some minor local roads. We also model 43 transit networks, as detailed in [17].

70 We model damage from ground shaking intensity to a set of 1743 highway bridges impacting the road and some
 71 transit networks, with data provided by the California Department of Transportation (Caltrans), and 1409 structures



Figure 1. Study area: San Francisco Bay Area, CA with specific travel analysis zones (TAZs) used in the case study marked in blue.

72 impacting the rapid transit network, BART, with data provided by that agency. We refer readers to [17] for more
 73 details about matching these structures, hereafter called components, to the relevant road and transit networks.

74 2.2. Ground-motion intensity maps

75 2.2.1. Theory

76 We now describe how to produce a set of maps with ground-motion intensity realizations at each location of
 77 interest in a region and corresponding occurrence rates that reasonably capture the joint distribution of the ground-
 78 motion intensity. First, we generate Q earthquake scenarios from a seismic source model. The seismic source model
 79 specifies the rates at which earthquakes of specified magnitudes, locations, and faulting types will occur. This set of
 80 earthquake scenarios is comparable to a stochastic event catalogue in the insurance industry.

81 Second, for each earthquake scenario in the seismic source model, we use an empirical ground-motion prediction
 82 equation (GMPE) [e.g., 20, 21, 22, 23] to model Y , the resulting intensity measure at each location of interest [e.g.,
 83 24, 25].

84 Then, for each of the Q earthquake scenarios, we sample b realizations of the spatially-correlated ground-motion
 85 intensity residual terms. Readers are referred to [26] for a survey of sampling methods. Once residuals are sampled,
 86 the total log ground-motion intensity (Y) is computed as

$$\ln Y_{ij} = \overline{\ln Y(M_j, R_{ij}, V_{s30,i}, \dots)} + \sigma_{ij}\epsilon_{ij} + \tau_j\eta_j \quad (1)$$

87 where j is the ground-motion intensity map index ($j = 1, \dots, m$ where $m = Q \times b$), ϵ_{ij} is the normalized within-event
 88 residual in $\ln Y$ representing location-to-location variability and η_j is the normalized between-event residual in $\ln Y$
 89 and the other parameters are defined above. Both ϵ_{ij} and η_j are normal random variables with zero mean and unit
 90 standard deviation. The vector of ϵ_{ij} can be modeled by a spatially-correlated multivariate normal distribution [e.g.,
 91 27] and the η_j by a standard univariate normal distribution.

92 The result is a set of m ground-motion intensity maps (e.g., Figure 2(a)). Since we simulate an equal number
 93 (b) of ground-motion intensity maps per earthquake scenario, the annual rate of occurrence for the j^{th} ground-motion
 94 intensity map is the original rate of occurrence of the earthquake scenario, divided by b . We denote the rate associated
 95 with the j^{th} ground-motion intensity map as w_j .

96 2.2.2. Implementation

97 To generate a stochastic catalog of ground-motion intensity maps, we use the OpenSHA Event Set Calculator [28].
 98 This software outputs the mean, $\ln Y_{ij}$, and standard deviation values, σ_{ij} and τ_j , for all locations of interest for a
 99 specified seismic source model and ground-motion prediction equation, which are needed inputs for Equation 1. The
 100 intensity measure is the 5%-damped pseudo absolute spectral acceleration (Sa) at a period $T = 1\text{s}$, which is the
 101 required input to the fragility functions below. This spectral acceleration value represents the maximum acceleration
 102 over time that a linear oscillator with 5% damping and a period of 1 second will experience from a given ground
 103 motion. We calculate these values at each component location (bridges and other structures). Using one ground-
 104 motion intensity measure per component is a common simplification of the time-varying acceleration dynamics [e.g.,
 105 29, 9] that may have lower errors for components with a natural period near 1 second as opposed to long-span bridges.
 106 We use the UCERF2 seismic source model [30], Wald and Allen topographic slope model for the shear wave
 107 velocity $V_{s30,i}$ [31], and the Boore and Atkinson [20] ground-motion prediction equation. Using this seismic source
 108 model, which is then discretized into a list of faults and a stratified list of magnitudes and rupture locations for each,
 109 we obtain a set of 2110 earthquake events on all active faults, each with an annual occurrence rate greater than or equal
 110 to 10^{-5} . We simulate the sets of maps by combining the mean terms from the Event Set Calculator and spatially-
 111 correlated residual terms of the ground-motion intensity (using [27]) according to the basic ground-motion model,
 112 Equation 1.

113 2.3. Damage maps

114 2.3.1. Theory

115 Calculating network performance risk requires assessing the structural damage of relevant components after future
 116 earthquakes. The link between ground-motion intensity and structural damage is often provided by fragility functions.
 117 Fragility functions express $P(DS_i \geq ds_i | Y_{ij} = y)$. We assume one component, such as a bridge, per site location, so we

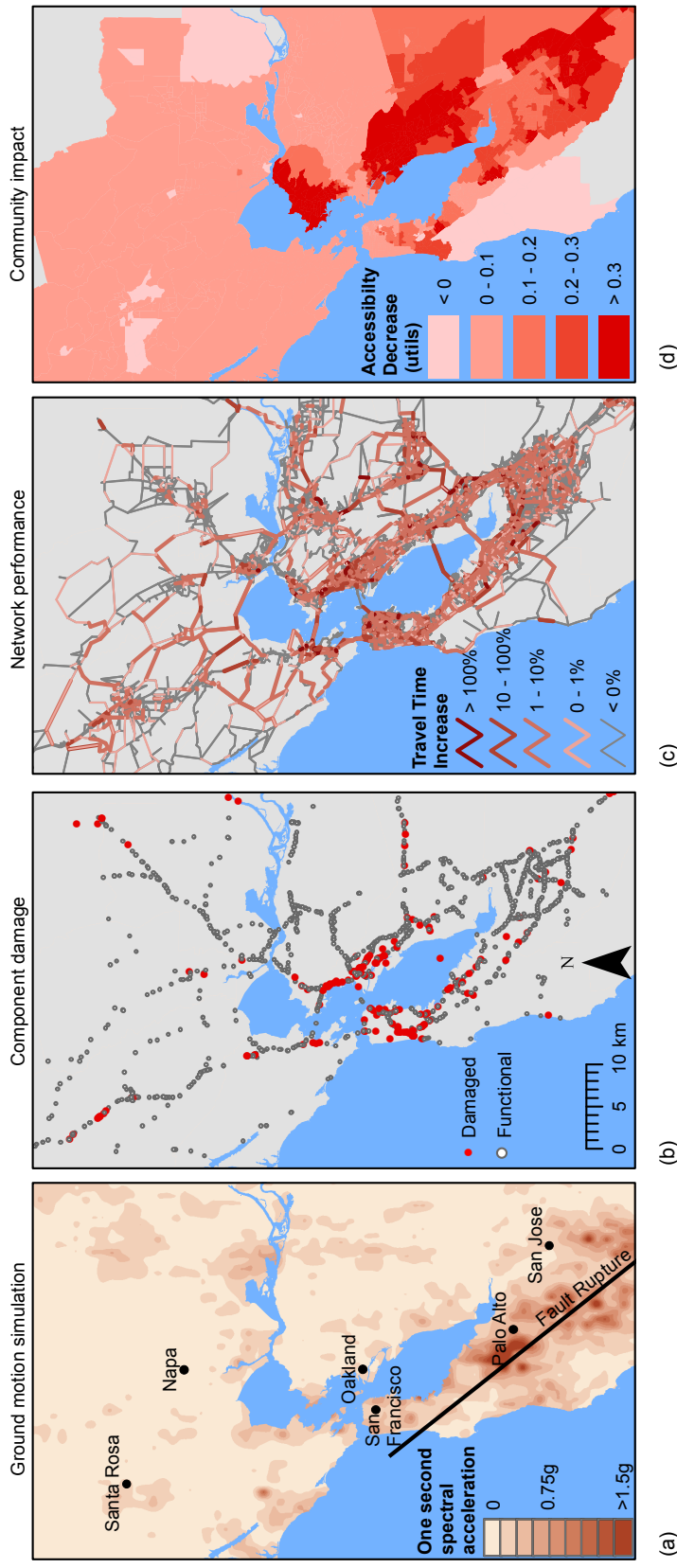


Figure 2. Illustration of the risk framework for one earthquake event including a) One-second spectral acceleration (ground-motion intensity) map with earthquake rupture, b) bridge (component) damage map, c) map of travel time increase (network-performance measure) values, and d) map of accessibility values averaged over all market segments by travel analysis zone (TAZ).

118 will identify both components and site locations via the index i . Using that notation, DS_i is a discrete random variable
 119 whose value represents the damage state for the i^{th} component and ds is a damage state threshold of interest. The
 120 damage state is conditioned on a realization, y , of the random variable Y_{ij} , the ground-motion intensity at the i^{th} site
 121 and j^{th} ground-motion intensity map. Researchers have calibrated fragility functions using historical post-earthquake
 122 data [e.g., 32], experimental and analytical results [e.g., 33], hybrid approaches, and expert opinion. It is possible to
 123 sample the damage states from a joint distribution that includes correlation, such as due to similarities in design or
 124 construction practices [e.g., 34].

125 By sampling a damage state for each component, with probabilities obtained from the fragility functions given
 126 the ground-motion intensity, we produce a damage map (e.g., Figure 2(b)). The damage map has a realization of the
 127 damage state of each relevant component. This sampling process can be repeated multiple times to simulate multiple
 128 damage maps per ground-motion intensity map. For example, if equal numbers of damage maps are sampled per
 129 ground-motion intensity map (c damage maps per ground-motion intensity map), the weight of the j^{th} damage map
 130 should be adjusted accordingly to w_j , where $w_j = \frac{w_j}{c}$, and $j' = 1, \dots, J$.

131 *Functional percentage* relationships link the component damage to the functionality of network elements. For
 132 example, in a road network, when a bridge collapses, the traffic flow capacity of the road it carries and it crosses
 133 can be modeled as reduced to zero. These relationships are typically derived from a combination of observation
 134 and expert opinion, often due to data scarcity [35]. Furthermore, the relationships are typically deterministic for a
 135 certain component damage state and restoration time [35]. Thus, in this paper, each damage map corresponds to a
 136 functionality state for every element of the network.

137 2.3.2. Implementation

138 *Component damage.* We use fragility functions of the following form to provide the link between ground-motion
 139 shaking and component damage:

$$P(DS_i \geq ds_s | Y_{ij} = y) = \Phi\left(\frac{\ln y - \lambda_{s,i}}{\xi_{s,i}}\right), \quad (2)$$

140 where Φ is the standard normal cumulative distribution function, $\lambda_{s,i}$ and $\xi_{s,i}$ are respectively the mean and standard
 141 deviation of the $\ln Y_{ij}$ value necessary to cause the s^{th} damage state to occur or be exceeded for the i^{th} component,
 142 and the other variables are defined above. By using the previous equation and the inverse method, we can sample
 143 realizations of component damage states for a given ground-motion intensity.

144 The California Department of Transportation (Caltrans) provided the fragility function values $\lambda_{s,i}$ and $\xi_{s,i}$ used
 145 in this study for the highway components in summer 2012, which was last updated in 2007 and includes various
 146 retrofitted bridges [36]. The $\lambda_{s,i}$ values are based on component characteristics including number of spans and age
 147 as detailed in [32]. The $\xi_{s,i}$ values are given as a constant. The BART seismic safety group provided the fragility
 148 function values $\lambda_{s,i}$ and $\xi_{s,i}$ used in this study for the BART-related components for the state of the network in summer
 149 2012. At that time, data was available for the aerial structures shown in Figure ???. These correspond to the safety
 150 performance goals under the recent retrofit program [37]. The numbers are comparable to the Caltrans fragility data.
 151 For the BART components, however, $\xi_{s,i}$, the standard deviation of the $\ln S_a$ value necessary to cause the extensive
 152 damage state to occur or be exceeded, varies depending on the component. Both sets of fragility functions are based
 153 on the assumption that damage can be reasonably accurately estimated by the ground motion intensity at each site
 154 independently, and that the damage state can be reasonably estimated by an analytical model considering a single
 155 ground-motion intensity measure. In addition, the fragility curves do not directly consider the effects of degradation.
 156 Current work is ongoing to refine these assumptions [e.g., 33, 38, 39].

157 Caltrans also provided other component properties such as length, construction year, construction materials, out-
 158 to-out distance (the maximum distance in the perpendicular direction to traffic flow), number of spans, and average
 159 daily traffic flow). Similarly, Caltrans provided estimates for bridge replacement costs in current (2014) USD: 175 per
 160 square foot for construction and 10 per square foot for demolition of the damaged bridge [40].

161 Per ground-motion intensity map, we sample 1 damage maps (e.g., Figure 2(b)), which each has a realization of
 162 the component damage state at each component location according to the fragility function (eq. 2). The provided
 163 fragility functions do not consider correlation of the structural capacities, but other models could be used [e.g., 34].

164 *Transit network damage.* Each of the 43 transit systems we considered will be impacted differently. For Caltrain,
 165 conversations with managers suggest that given that there is one shared track system, the system would either be

166 fully operational or not at all. Similarly, managers suggested modeling the VTA system as fully functional or not.
 167 Depending on where the BART train cars are when the earthquake strikes, the agency could accommodate different
 168 emergency plans. However, BART representatives suggested considering that if any part of a route is damaged, the
 169 entire corresponding route would not be operational (but other routes on different tracks might be still operational). In
 170 other words, each BART route as well as the Caltrain and VTA routes are each a weakest-link system, so the failure
 171 of a single component will cause the route to be non-operational. We modeled the ferry systems as fully functioning
 172 for all earthquake events. For all earthquake events including the baseline, trans-bay and cross-county bus lines were
 173 discontinued, but main lines in urban areas as well as other local bus networks were maintained per recommendations
 174 from the MTC, though they may face delays due to traffic congestion.

175 *Road network damage.* Each component damage state maps directly to the traffic capacity on associated road seg-
 176 ments. We use a functional percentage relationship to compute the traffic capacity of relevant road segments. Based
 177 on discussions with Caltrans, we consider travel conditions one week after an earthquake, since it is a critical period
 178 for decision making. For example, one week after most events, bridges should have been inspected and surface dam-
 179 age should be repaired, but major reconstruction would not have yet begun. According to our functional percentage
 180 relationship, at this point in time, the components have one of two classes of functionality, zero traffic capacity and
 181 full traffic capacity [35]. We can thus summarize the component damage using two damage states ds_s , $ds_{damaged}$ and
 182 $ds_{functional}$, which correspond to the common HAZUS *extensive* or *complete* damage states and the *none*, *slight*, or
 183 *moderate* damage states respectively [35]. Thus, the functional percentage relationship assigns zero traffic capacity
 184 on road segments that have at least one component in the $ds_{damaged}$ damage state, and full traffic capacity otherwise.
 185 We do not consider network damage from sources other than main structural damage from ground shaking, such as
 186 tunnel displacement or liquefaction, but the framework allows including such considerations. In the discussion below,
 187 we consider a set of 113,940 damage maps, which correspond to 2110 scenarios, 3 ground-motion intensity maps per
 188 scenario, and 18 damage maps per ground-motion intensity map.

189 2.4. Network performance

190 2.4.1. Theory

191 The final step for the event-based risk analysis is to evaluate the network performance measure, X . For this
 192 application, we consider a metric popular in urban planning, *mode-destination accessibility change* [e.g., 15, 41, 42]
 193 (e.g., Figure 2(d)). Mode-destination accessibility, hereafter referred to as accessibility, measures the distribution of
 194 travel destination opportunities weighted by the composite utility of all modes of travel to those destinations, i.e.,
 195 the ease of someone getting to different destinations weighted by how desirable those destinations are [16, 14]. The
 196 utility function for the mode-destination choice may be estimated using a multinomial random utility model where
 197 the logsum represents the accessibility value [43, 16, 14]. Namely, accessibility for a particular agent a is

$$Acc_a = \ln \left[\sum_{v \in C_a} \exp(V_{a(c)}) \right], \quad (3)$$

198 where $V_{a(c)}$ is the utility of the c^{th} choice for the a^{th} person for $a = 1, \dots, A$, and C_a is the choice set for the a^{th}
 199 person [16]. Choices refer to travel destinations and the mode of travel (driving, walking, bus, etc.). The units are a
 200 dimensionless quantity, *utils*. As an extension, the accessibility values from the previous equation can be converted
 201 into equivalent time and dollar amounts using *compensating variation* for cost-benefit studies; for the case study,
 202 0.0134 *utils* (generic measure of utility) equals the value of one minute per day [14, 44, 45] and we conservatively
 203 value one hour of time as approximately \$15 [46]. In other words, one *util* is worth approximately \$20 per person per
 204 day based on these assumptions. With nearly 7 million people in the region, even small changes in *utils* lead to large
 205 economic losses. Since accessibility measures how easily people can get to the destinations they desire, accessibility
 206 is used as one of the measures of human welfare [e.g., 14].

207 Once the chosen performance measure is computed for each damage map, we aim to estimate the exceedance
 208 rate of different levels of performance. The annual rate, λ , of exceeding some threshold of network performance
 209 is estimated by summing the occurrence rates of all damage maps in which the performance measure exceeds the

210 threshold:

$$\lambda_{X \geq x} = \sum_{j'=1}^J w_{j'} \mathbb{I}(X_{j'} \geq x) \quad (4)$$

211 where x is an accessibility value threshold of interest and $X_{j'}$ is the accessibility value realization for the j'^{th} damage
 212 map. The variable $w_{j'}$ is the occurrence rate of the j'^{th} damage map. The indicator function \mathbb{I} evaluates to 1 if the
 213 argument, $X_{j'} \geq x$, is true, and 0 otherwise. By evaluating λ at different threshold values, we derive an exceedance
 214 curve (e.g., Figure 6).

215 **2.4.2. Implementation**

216 We compute accessibility using *Travel Model One* (version 0.3), an activity-based model used by the Metropolitan
 217 Transportation Commission (MTC), the local metropolitan planning organization (MPO) [47]. It represents the full
 218 road network as well as the public transit networks, biking, and walking. Travel demand data consists of the locations
 219 of different households in the case study area, their destination preferences and utilities, their number of vehicles,
 220 their income and other demographic data [47, 45]. More details can be found in [48]. This data was collected by
 221 the MTC from surveys and census information. We assume that the distributions of travel preferences do not change
 222 after an earthquake, although the actual destinations and trips may vary. For example, if a trip takes a very long time
 223 after a simulated earthquake, it is less likely that the trip will occur. The result is a *variable* travel demand model.
 224 This model uses a combination of Java code called CT-RAMP [49], and the Citilabs Cube Voyager and Cube Cluster
 225 software programs, which are part of a leading commercial software suite for transportation planning [47]. This model
 226 differs from previous representations of this network [e.g., 9, 50], since it includes not only major roads but also local
 227 roads and transit lines. We have provided further details about computing mode-destination accessibility using this
 228 high-fidelity model in [17].

229 This analysis considers 40 interesting and hazard-consistent events, as defined by 40 sets of ground-motion inten-
 230 sity maps, damage maps, and accessibility performance measure realizations. We selected this set of events with the
 231 optimization-based procedure we introduced in [18]. Readers are referred to [17] for more details about this set of
 232 events.

233 In the following sections, we first compare region-wide results, and then focus on particular characteristics of
 234 three communities (Figure 1 shows the study area and three communities). Finally, we discuss generalizable trends.

Income class	Income range, 1989 USD	Income range, 2014 USD
Low	0 - \$25,000	0 - \$47,334
Medium	\$25,000 - \$45,000	\$47,334 - \$85,202
High	\$45,000 - \$75,000	\$85,202 - \$142,004
Very high	more than \$75,000	more than \$142,004

Table 1. Income class definitions for the case study region, as defined by the local planning organization, the MTC [45] and also translated to current 2014 USD using the consumer price index.

235 3. Results and Discussion

236 3.1. Overview of results region-wide

237 In this section, we analyze region-wide trends in accessibility losses for the case study area. As mentioned in
 238 Section 1, we first analyze each of the 12 socio-economic groups used in practice for the case study region [45], which
 239 are characterized based on households. The socio-economic groups correspond to all combinations of four different
 240 income classes (Table 1), and three different classes of automobile availability in the household (zero automobiles,
 241 fewer automobiles than household members that work, a greater or equal number of automobiles as compared to the
 242 number of household members that work).

243 We first assess the data availability for each of the segments. Each data point represents a trip by a person of a
 244 household, who is modeled as an agent in the high-fidelity transportation model. The results suggest comparing house-
 245 holds with at least one car, because for households without cars (no cars), only the low income class has reasonably
 246 many trips.

247 General patterns emerge in the expected losses in accessibility. The expected losses are computed by taking
 248 an average of the accessibility results for each of the 1454 travel analysis zones (TAZ) for each earthquake event,
 249 weighted by the adjusted annual likelihood of occurrence from the optimization results.

250 First, we notice that the ratio of cars to the number of people who work in a household is correlated with accessi-
 251 bility risk; a higher ratio corresponds to higher expected decreases in accessibility. This corresponds to going across a
 252 column in Figure 3. For example, for the first row representing low income households, we notice a marked change in
 253 accessibility across the columns, as indicated by an expanded area of darkened TAZs from left to right (Figure 3(a-c)).
 254 Note that 1 *util* corresponds to a consumer value of compensating variation of approximately \$20 per person per day,
 255 which assumes low (conservative) estimates of the value of time for travel delays and value of getting to destinations.

256 We might expect these households with more cars to take longer trips because there might be a relationship
 257 between needing to travel longer distances and needing an extra car or two in a household. This is indeed the case,
 258 but it is not fully predictive. In fact, there is only a weak trend between average trip length for a TAZ before any
 259 earthquake and the predicted impact on accessibility (Figure 4). Instead, we hypothesize that there are other latent
 260 variables correlated with car ownership. For example, the geographic distribution of people without cars varies.
 261 Additionally, in Section 3.5, we will further explore the correlation between the percentage of car-based trips and
 262 accessibility risk. We will show that TAZs with fewer car-based trips, tend to have lower risk of accessibility losses.

263 Second, controlling for car ownership, we see a fairly equitable distribution of risk across income class segments.
 264 For example, by looking at households with fewer workers than cars (middle column of Figure 3), the variation from
 265 TAZ to TAZ is significantly more striking than the difference across income segments (Figure 3(b,e,h,k)). Similarly,
 266 while trip lengths are slightly longer for higher income households, the differences are subtle.

267 Thus, for a given TAZ, the differences across incomes are not that great. At the same time though, there is
 268 an unequal geographic distribution of wealth in the San Francisco Bay Area. Because of this, when we aggregate
 269 accessibility risk across TAZs, we see that accessibility risk rises with increasing household income (Figure 6(b)).
 270 Therefore, even though the poor are generally the most vulnerable to natural disasters including hurricanes, floods
 271 and earthquakes, wealthier households in the San Francisco Bay area are more vulnerable than the other income
 272 groups to earthquake-related accessibility risk.

273 Next, we consider which geographic parts of the San Francisco Bay Area are at an elevated risk. The results show
 274 regions of high risk: in the East Bay due East of San Francisco, in the suburbs of San Jose, along the coastal and
 275 Bay-side regions South of San Francisco (Millbrae and Pacifica, e.g.), and in parts of San Francisco (South-Central
 276 neighborhoods including Westland Highlands and Glen Park neighborhoods). One may have expected more high risk

areas on the San Francisco Peninsula, because of the San Andreas fault, which can generate large magnitude events. In contrast, the East Bay has higher shaking levels at more moderate return periods, due to the higher relative annual frequency of events on the Hayward Fault; this is correlated to bridge damage and thus road closures. Furthermore, the data suggests that both the more common moderate-magnitude East Bay events and the rare higher-magnitude San Andreas events can cause accessibility problems for the East Bay. Figure 5 shows one sample realization of a M6.85 Hayward event and one sample realization of a M7.45 San Andreas event—both follow the general trend of high predicted accessibility losses in the East Bay. In contrast, while any events could contribute to the risk in San Francisco, our model results show the main accessibility losses in San Francisco corresponding to the San Andreas events. Figures 5(c,d) provide one such example. Figures 5(e,f) show an example of a lower magnitude event farther away from the main population centers, a M6.35 event in the Great Valley Pittsburg-Kirby Hills Fault. This shows how the range of more minor faults in the East Bay can contribute to that area's risk. Also, we have shown the results for one socio-economic group in Figure 5, but the other socio-economic groups follow the same general patterns, albeit with different specific values.

Finally, we can examine the rates of loss exceedance (Equation 4). Figure 6 shows a similar shape to the loss exceedance curves for other metrics such as portfolio losses and travel time delay [17]. Note that the results are primarily valid in the 100 to 2475 year return periods, since this is the range chosen for the map selection optimization problem. Recognizing that the impact varies significantly by TAZ, as indicated by Figure 3, we also examine the accessibility loss exceedance curve for three communities: part of the San Francisco financial district, Danville, and Pacifica (Figure 1). These correspond to TAZ IDs 2, 1161, and 224 respectively. This part of the San Francisco financial district represents an area with relatively low expected changes in accessibility (Figure 3), whereas Danville and Pacifica are at an elevated risk in almost all socio-economic groups (Figure 3). The general trends are corroborated by the loss exceedance curves for these three communities (Figure 6(a) shows an example for the socio-economic group with medium income households with fewer cars than workers). In other words, the average middle-class person from Danville in a household with fewer cars than people who work is expected to experience travel-related losses up to 1 *utils* per day after a rare earthquake, which he or she values at approximately \$20 per day considering a conservative estimate of travel time and destination value. In contrast, his or her fellow Bay Area resident in San Francisco has expected losses of only a tenth as much as experienced by a Danville resident. At return periods greater than 100 years, we notice that Danville and Pacifica follow a similar general pattern, which differs dramatically from that of San Francisco.

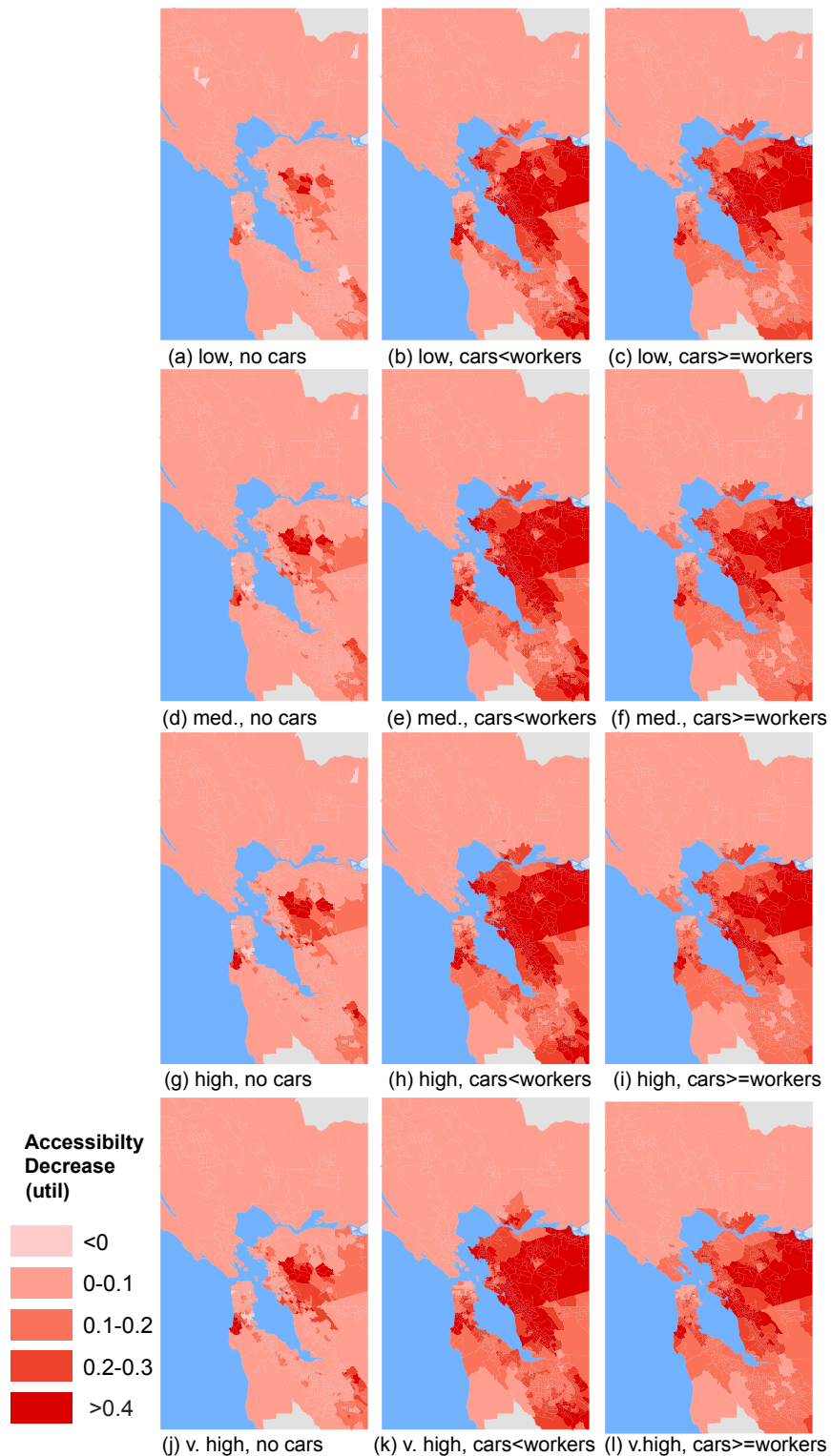


Figure 3. Expected changes in accessibility per person per day for each combination of income class and car ownership group. The darker the color, the greater the losses in accessibility.

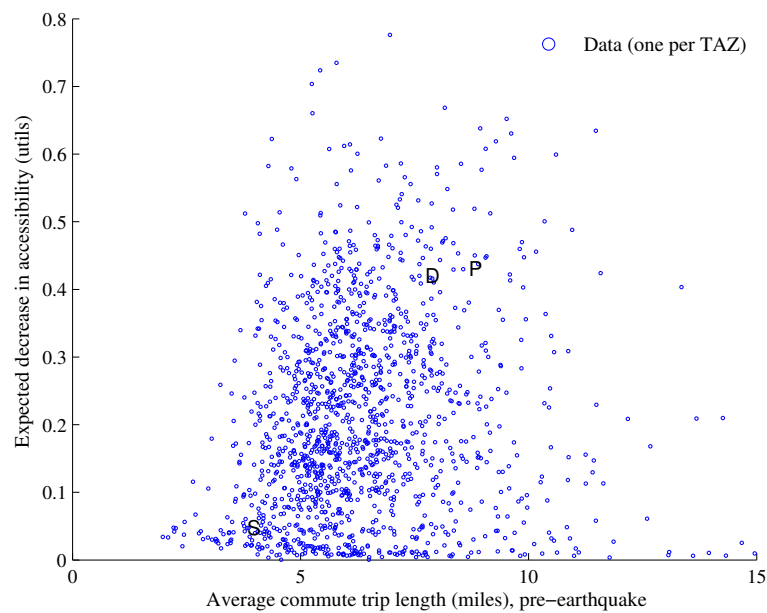


Figure 4. Trip length (pre-earthquake) versus change in total accessibility per person per day. Each dot represents one TAZ and the three case study communities, San Francisco financial district, Danville, and Pacifica are marked by **S**, **D**, and **P** respectively.

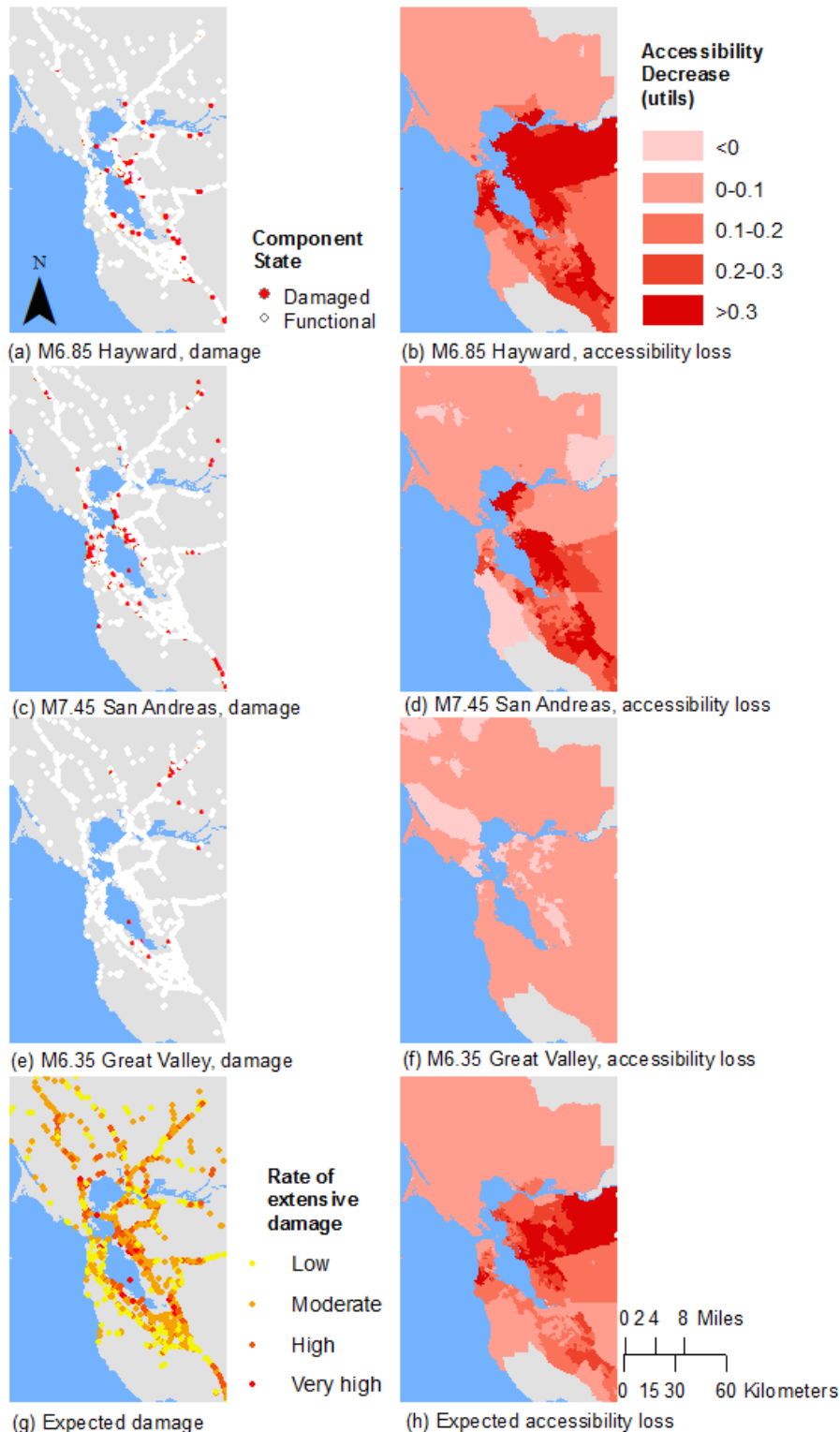


Figure 5. Bridge damage (red = damaged) and corresponding accessibility losses per person per day by TAZ for medium income households with fewer cars than workers. The bottom row has expected values calculated as a weighted average over all events.

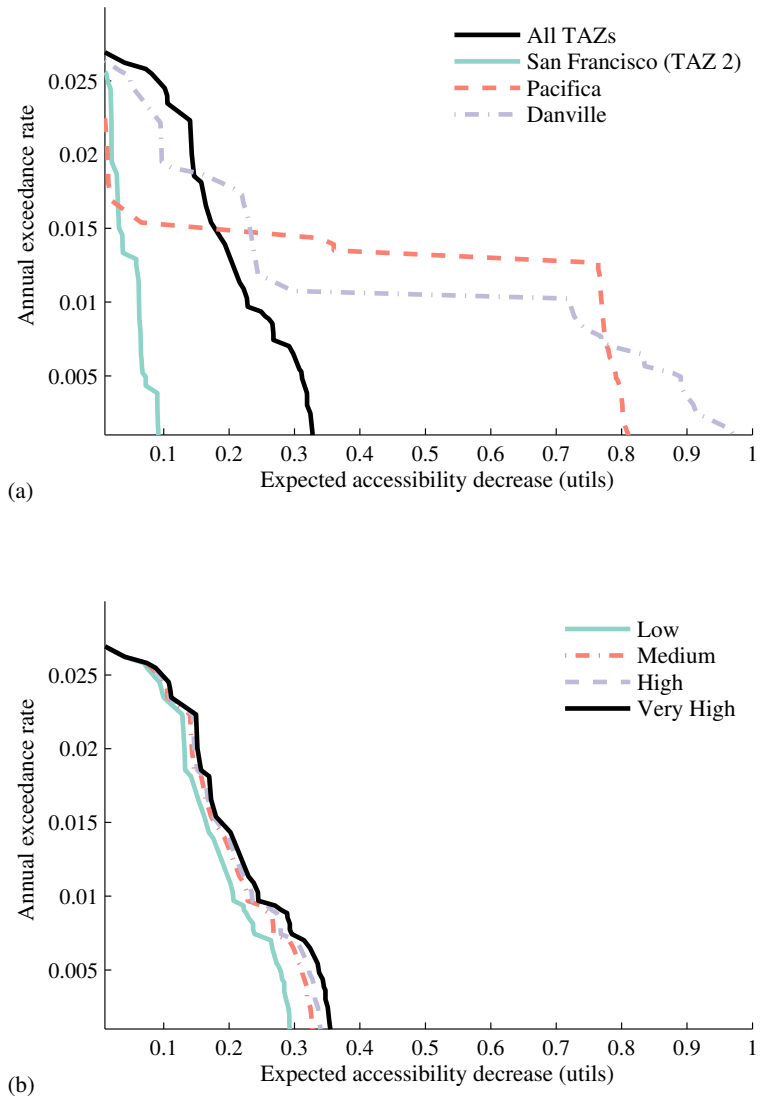


Figure 6. Accessibility annual loss exceedance curve with a comparison by (a) case study TAZs and average over all TAZs and (b) income class; all curves are in *utils* per person per day for medium income households with fewer cars than workers .

306 ***3.2. Analysis for San Francisco, CA financial district***

307 In this section, we will explore some possible explanations for why this San Francisco TAZ (Figure 1) has lower
 308 expected accessibility losses than most other communities. First, the financial district of San Francisco differs dramatically
 309 from many other TAZs in that the percentage of trips made by car is relatively small (38% versus an average of
 310 85% across all TAZs). Households traveling by foot or bike will be less influenced by network damage, because the
 311 model considers only damage to the road network and transit systems; thus, foot travel routes and travel times will not
 312 be affected in this model. We also observe that more trips by foot and bike correspond to destinations that are closer
 313 geographically. The impact of travel mode shift post-earthquake will be further explored in Section 3.5.

314 Second, the average time for a trip to and from work is about average for a TAZ in this region and also follows
 315 a similar distribution to that of the other TAZs; the average trip distance for trips is only 7% lower than the average
 316 for all trips region-wide. Since the trip time and length are relatively typical, but the accessibility is much lower than
 317 average, the trip time and length do not explain the differences in accessibility losses.

318 In summary, the data suggests that a major cause for the low expected accessibility impact for the financial
 319 district of San Francisco is the lower relative dependence on cars for mobility. In the next section, we will contrast
 320 the San Francisco example with results from Pacifica, another Peninsula community that, nonetheless, is expected to
 321 be at high risk of losses in accessibility.

322 ***3.3. Analysis for Pacifica, CA***

323 We might not suspect that Pacifica, CA would be at an extremely elevated risk of accessibility losses across most
 324 market segments, as compared to other communities, because it is not unusually close to a major earthquake fault.
 325 In addition, the percentage of pre-earthquake car-based trips is around average for the case study area (88% versus
 326 an average of 85%). In contrast to most other regions, however, Pacifica is wedged between the Pacific Ocean to
 327 the West and the coastal mountains to the East. Indeed, the main access road is California Highway 1, which has
 328 various vulnerable bridges included in the case study dataset. There are no viable alternative routes on local roads.
 329 Since almost all trips are by car from Pacifica and the average trip length is much longer than the region-wide average
 330 (108% longer), the road issue is particularly serious.

331 As a comparison, consider the next main town along the Pacific coast, Half Moon Bay, about 13 miles South. Half
 332 Moon Bay has significantly lower expected accessibility losses compared to Pacifica (0.11 *utils* per day for a person
 333 in Half Moon Bay in middle income household with fewer cars than workers, given an event in the dataset, versus
 334 0.43 *utils* per day for a similar person in Pacifica). While the seismic hazard is similar, the population is about one
 335 third the size, so there is less demand for the limited road capacity [51]. Furthermore, and likely most significantly,
 336 Half Moon Bay has a key alternative to California Highway 1, California Highway 92, which links to Silicon Valley
 337 and the main highways of that region (US-101 and I-280). Since Pacifica, CA is unusually reliant on one road with
 338 key vulnerabilities for access, it has an elevated risk for losses in accessibility.

339 ***3.4. Analysis for Danville, CA***

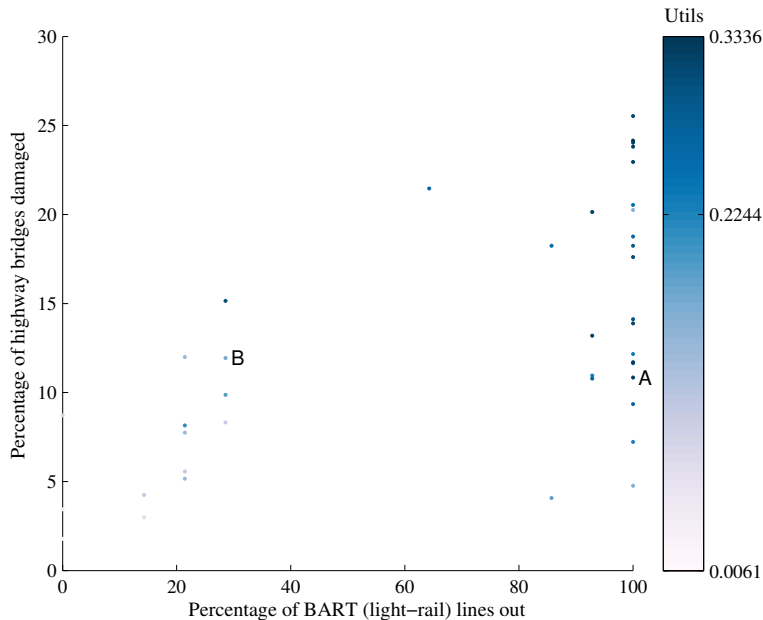
340 We will first examine the trip length characteristics for Danville, CA. The distribution of pre-earthquake commute
 341 trips from Danville, CA is shifted towards both longer distance and longer time than the communities we have studied
 342 so far, with a relatively higher proportion of trips taking 60–74 minutes and traveling over 40 miles than in the other
 343 communities. The same trend holds for other trip purposes. On average, the trip lengths are longer than many other
 344 TAZs (85% longer than the average over all trips originating from any of the TAZs). The consequence of these longer
 345 trips is more opportunities to be impacted by a road closure, simply because more roads and bridges will be used.
 346 Moreover, the road layout near Danville, CA mandates many highway trips, which increase the likelihood of crossing
 347 bridges; bridges are the part of the network for which we model the vulnerability.

348 Next, we look at patterns of expected bridge damage. Bridge damage is important for many regions, including
 349 Danville, because the percentage of car-based trips is high (85% of all trips on average, and also 85% of Danville-
 350 origin trips). For damage map realizations for the three earthquake events we introduced—M6.85 Hayward Fault,
 351 M7.45 San Andreas Fault, M6.35 Great Valley Fault—some bridges in the Oakland area are in the extensive or
 352 greater damage state (Figure 5(a,c,e)). These correspond to bridge closures in the model. In addition, in the first two
 353 cases, there are closures to the north of Danville, which represents one of the two main travel routes from Danville.
 354 There are also scattered closed bridges to the west of Danville, likely a top travel corridor because of the workplace

355 centers in San Francisco, Oakland, and Silicon Valley (all to the west). As for transit, in the first two events, all BART
 356 lines are closed, so there are limited alternatives to the popular road routes. The result is that the residents of Danville,
 357 CA have reduced access to their normal destinations after all these events.

358 We can also look at bridge damage in a probabilistic event-set-based manner. The expected damage over all
 359 events represents the annual rate of a bridge being in the extensive or complete damage state for the set of 113,940
 360 damage maps (Figure 5(g)). This figure indicates that bridges in the Oakland-Berkeley area are particularly likely to
 361 be damaged. We also see a few high likelihood bridges to the North of Danville. Thus, the data suggests that the
 362 relative position of high-risk bridges to Danville contributes to this community's accessibility risk.

363 *3.5. Impact of travel mode shifts and regional variations in travel mode patterns*



Functionality	BART	Caltrain	Muni Light Rail	VTA Light Rail
Full	3	13	25	9
50-99%	10	0	15	0
1-49%	8	0	0	0
None	19	27	0	31

Table 2. Transit network functionality as a count out of the forty simulated events for BART, Caltrain, Muni Light Rail, and VTA Light Rail. Functionality is measured by the percentage of lines that are operational given a damage map (based on a ground-motion intensity map).

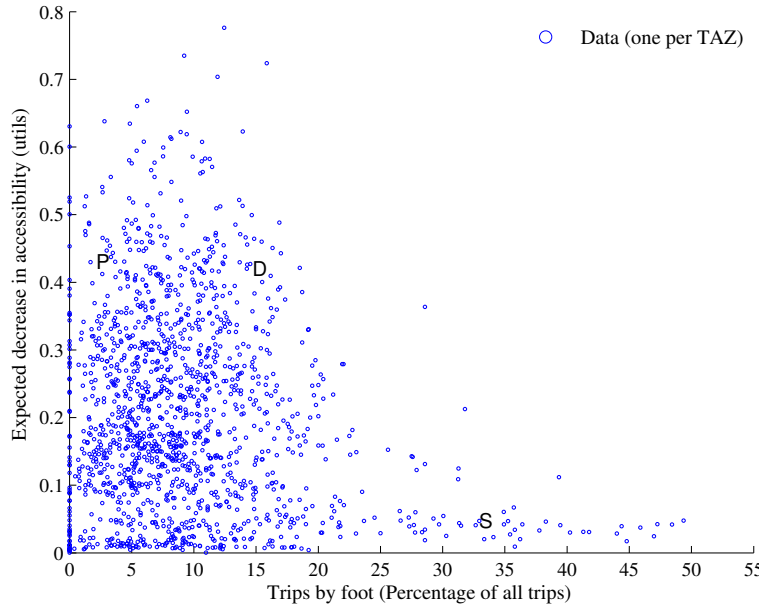


Figure 8. Percentage of total trips by foot (pre-earthquake) versus decrease in total accessibility, measured in *utils* per day (for households with the number of cars less than the number of workers). Each dot represents one TAZ and the three case study communities, San Francisco financial district, Danville, and Pacifica are marked by S, D, and P respectively.

forty events analyzed with the high-fidelity model, the M6.85 Hayward Rogers-Creek and the M7.45 Northern San Andreas Fault event both have a similar number of damaged bridges (around 11%); these are noted by points A and B respectively in Figure 7. These correspond to the bridge damage and accessibility maps in Figures 5(a,b) and 5(c,d) respectively. However, this Hayward Rogers-Creek event has significantly higher accessibility impact. Similarly, the transit impact was different. This Northern San Andreas event had only 4 of the 14 BART lines, all Caltrain, and all VTA Light Rail lines not operational, whereas this Hayward Rogers-Creek event had all 14 of the 14 BART lines, all Caltrain, all VTA Light Rail and 3 of the 8 Muni light rail lines not operational. Thus, the transit lines were impacted significantly differently. Moreover, the differences in accessibility results could not have been predicted from simpler models focusing on bridge portfolio losses, because the percent of damaged bridges was about the same, and the San Andreas event actually corresponded to a greater increase in travel time.

Second, we examine the correlation between a community's walkability, as measured by the percentage of total trips made by that travel mode, and the expected decrease in accessibility by community. We see that an increased percentage of pre-earthquake trips on foot corresponds to a lower average decrease in accessibility (Figure 8). This result corroborates the specific example of the San Francisco Financial District we saw in Section 3.2. Furthermore, on average, the number of by-foot trips slightly increases after the earthquake events where road congestion worsens. This model result is consistent with the observations after the 1995 Kobe earthquake, in which many commuters switched to walking and biking ("non-mechanized modes") in the weeks after the earthquake [7]. In conclusion, the data suggests that TAZs, i.e. communities, which have a greater walkability are also more resilient to earthquake-related accessibility risk.

399 **4. Conclusions**

400 Here we have shown how mode-destination accessibility links post-earthquake infrastructure damage to the impact
 401 on human welfare and enables identifying at-risk geographic and demographic groups in a region. Adopting this
 402 state-of-the-art performance metric from the urban planning community, we have illustrated its use for seismic risk
 403 assessment and mitigation through a case study of the San Francisco Bay Area. For the case study, we consider a
 404 set of 40 hazard-consistent earthquake scenarios, ground-motion intensity maps, and damage maps. For each damage
 405 map, we processed the data for analysis in a high-fidelity, activity-based travel model that includes the road network,
 406 transit networks, walking and biking options, variable travel demand, and mode choice. We used this data and model
 407 to compute the mode-destination accessibility, a performance measure for each community and each socio-economic
 408 group (defined by income class and car ownership).

409 We saw stark differences in accessibility from location to location. Specifically, we found that areas in the suburbs,
 410 such as the far East Bay, South San Jose and select communities just south of San Francisco, were particularly at risk.
 411 We found that these geographic trends persisted across income classes and car ownership groups. Nonetheless, on
 412 average, higher income households with more cars than workers had the highest risk across the studied socio-economic
 413 groups. One key reason is the geographic clustering of these households in higher-risk areas. Another factor is that
 414 these households tend to take longer daily trips, thus crossing more roads and bridges and possibly increasing the
 415 likelihood of disruption.

416 This study also demonstrated that travel modes shift after an earthquake, and communities who can more easily
 417 make these adjustments are generally predicted to experience lower post-earthquake losses in accessibility. The results
 418 suggest that the walkability of a community, as measured by the percentage of pre-earthquake trips by foot, is closely
 419 linked to reduced accessibility risk. We also found that one adaptation measure after major earthquakes is an increased
 420 likelihood to walk or bike. We also found that in almost all of the simulated earthquake events, the transit system,
 421 particularly the heavy rail (BART and Caltrain) lines, is predicted by this model to be severely impacted. The result
 422 is a reduced mode share for transit and increased trips by the other modes (car, walk, bike). Thus, this study suggests
 423 that not including transit can lead to an unconservative estimate of seismic risk of transportation systems. The model
 424 shows, however, that when transit is not damaged—which is very rare for this case study—ridership increases.

425 In conclusion, mode-destination accessibility offers important applications for further investigation into the impact
 426 to human welfare of engineering losses and mitigation efforts. This work lays the foundation for future work in risk
 427 mitigation and policy to reduce the vulnerability of at-risk communities. It also suggests that initiatives making
 428 communities more conducive for cycling and walking to work can increase resiliency.

429 **References**

- 430 [1] L. Dueñas-Osorio, J. I. Craig, B. J. Goodno, Seismic response of critical interdependent networks, *Earthquake Engineering & Structural*
 431 *Dynamics* 36 (2) (2007) 285306. doi:10.1002/eqe.626.
- 432 [2] S. E. Chang, M. Shinozuka, J. E. Moore, Probabilistic earthquake scenarios: Extending risk analysis methodologies to spatially distributed
 433 systems, *Earthquake Spectra* 16 (3) (2000) 557–572. doi:10.1193/1.1586127.
- 434 [3] R. C. Bolin, L. Stanford, *The Northridge earthquake: vulnerability and disaster*, Routledge, London; New York, 1998.
- 435 [4] The World Bank and the United Nations, *Natural hazards, unnatural disasters: the economics of effective prevention*, Tech. rep., The World
 436 Bank, Washington D.C. (2010).
- 437 [5] California. Dept. of Transportation. Post Earthquake Investigation Team, *Northridge earthquake, 17 January 1994: PEQIT report*, California
 438 Department of Transportation, Division of Structures, Sacramento, 1994.
- 439 [6] K. J. Tierney, Business Impacts of the Northridge Earthquake, *Journal of Contingencies and Crisis Management* 5 (2) (1997) 87–97.
 440 doi:10.1111/1468-5973.00040.
- 441 [7] P. Gordon, H. W. Richardson, B. Davis, Transport-related impacts of the Northridge earthquake, National Emergency Training Center, 1998.
- 442 [8] A. Kiremidjian, J. Moore, Y. Y. Fan, O. Yazlali, N. Basöz, M. Williams, Seismic risk assessment of transportation network systems, *Journal*
 443 *of Earthquake Engineering* 11 (3) (2007) 371–382. doi:10.1080/13632460701285277.
- 444 [9] N. Jayaram, J. W. Baker, Efficient sampling and data reduction techniques for probabilistic seismic lifeline risk assessment, *Earthquake*
 445 *Engineering & Structural Dynamics* 39 (10) (2010) 1109–1131. doi:10.1002/eqe.988.
- 446 [10] C. S. Oliveira, M. A. Ferreira, F. M. d. S., The concept of a disruption index: application to the overall impact of the July 9, 1998 Faial
 447 earthquake (Azores islands), *Bulletin of Earthquake Engineering* 10 (1) (2012) 7–25. doi:10.1007/s10518-011-9333-8.
- 448 [11] P. Bocchini, D. M. Frangopol, Restoration of bridge networks after an earthquake: Multicriteria intervention optimization, *Earthquake Spectra*
 449 28 (2) (2012) 426–455. doi:10.1193/1.4000019.
- 450 [12] F. Cavalieri, P. Franchin, P. Gehl, B. Khazai, Quantitative assessment of social losses based on physical damage and interaction with infrastruc-
 451 tural systems, *Earthquake Engineering & Structural Dynamics* 41 (11) (2012) 1569–1589. doi:10.1002/eqe.2220.
- 452 [13] F. S. Chapin, *Urban land use planning*, University of Illinois Press, 1970.

- [453] [14] D. A. Niemeier, Accessibility: an evaluation using consumer welfare, *Transportation* 24 (4) (1997) 377396.
- [454] [15] K. T. Geurs, B. van Wee, Accessibility evaluation of land-use and transport strategies: review and research directions, *Journal of Transport Geography* 12 (2) (2004) 127–140. doi:10.1016/j.jtrangeo.2003.10.005.
- [455] [16] S. L. Handy, D. A. Niemeier, Measuring accessibility: an exploration of issues and alternatives, *Environment and Planning A* 29 (7) (1997) 11751194.
- [456] [17] M. Miller, Seismic risk assessment of complex transportation networks, PhD thesis, Stanford University (2014).
- [457] [18] M. Miller, J. Baker, Ground-motion intensity and damage map selection for probabilistic infrastructure network risk assessment using optimization, in review (2014).
- [458] [19] R. Cervero, K.-L. Wu, Polycentrism, commuting, and residential location in the San Francisco Bay area, *Environment and Planning A* 29 (5) (1997) 865–886.
- [459] [20] D. M. Boore, G. M. Atkinson, Ground-motion prediction equations for the average horizontal component of PGA, PGV, and 5%-damped PSA at spectral periods between 0.01 s and 10.0 s, *Earthquake Spectra* 24 (1) (2008) 99–138.
- [460] [21] N. Abrahamson, W. Silva, Summary of the Abrahamson & Silva NGA Ground-Motion Relations, *Earthquake Spectra* 24 (1) (2008) 67–97. doi:10.1193/1.2924360.
- [461] [22] B. Chiou, R. R. Youngs, An NGA model for the average horizontal component of peak ground motion and response spectra, *Earthquake Spectra* 24 (1) (2008) 173–215. doi:10.1193/1.2894832.
- [462] [23] K. W. Campbell, Y. Bozorgnia, NGA ground motion model for the geometric mean horizontal component of PGA, PGV, PGD and 5% damped linear elastic response spectra for periods ranging from 0.01 to 10s, *Earthquake Spectra* 24 (1) (2008) 139–171. doi:10.1193/1.2857546.
- [463] [24] J. W. Baker, C. A. Cornell, Which spectral acceleration are you using?, *Earthquake Spectra* 22 (2) (2006) 293–312. doi:10.1193/1.2191540.
- [464] [25] R. Foulser-Piggott, P. J. Stafford, A predictive model for Arias intensity at multiple sites and consideration of spatial correlations, *Earthquake Engineering & Structural Dynamics* 41 (3) (2012) 431451. doi:10.1002/eqe.1137.
- [465] [26] Y. Han, R. A. Davidson, Probabilistic seismic hazard analysis for spatially distributed infrastructure, *Earthquake Engineering & Structural Dynamics* 41 (15) (2012) 2141–2158. doi:10.1002/eqe.2179.
- [466] [27] N. Jayaram, J. W. Baker, Correlation model for spatially distributed ground-motion intensities, *Earthquake Engineering & Structural Dynamics* 38 (15) (2009) 1687–1708. doi:10.1002/eqe.922.
- [467] [28] E. H. Field, T. H. Jordan, C. A. Cornell, OpenSHA: a developing community-modeling environment for seismic hazard analysis, *Seismological Research Letters* 74 (4) (2003) 406 – 419. doi:10.1785/gssrl.74.4.406.
- [468] [29] M. Shinozuka, Y. Murachi, X. Dong, Y. Zhou, M. J. Orlikowski, Effect of seismic retrofit of bridges on transportation networks, *Earthquake Engineering and Engineering Vibration* 2 (2) (2003) 169–179. doi:10.1007/s11803-003-0001-0.
- [469] [30] E. H. Field, T. E. Dawson, K. R. Felzer, A. D. Frankel, V. Gupta, T. H. Jordan, T. Parsons, M. D. Petersen, R. S. Stein, R. J. Weldon, C. J. Wills, Uniform California Earthquake Rupture Forecast, Version 2 (UCERF 2), *Bulletin of the Seismological Society of America* 99 (4) (2009) 2053 –2107. doi:10.1785/0120080049.
- [470] [31] D. J. Wald, T. I. Allen, Topographic slope as a proxy for seismic site conditions and amplification, *Bulletin of the Seismological Society of America* 97 (5) (2007) 1379–1395. doi:10.1785/0120060267.
- [471] [32] N. Basöz, J. Mander, Enhancement of the highway transportation lifeline module in HAZUS, Tech. rep., Final Pre-Publication Draft (#7) prepared for the National Institute of Building Sciences (NIBS) (1999).
- [472] [33] K. N. Ramanathan, Next generation seismic fragility curves for California bridges incorporating the evolution in seismic design philosophy, PhD thesis, Georgia Institute of Technology (2012).
- [473] [34] R. Lee, A. S. Kiremidjian, Uncertainty and correlation for loss assessment of spatially distributed systems, *Earthquake Spectra* 23 (4) (2007) 753–770. doi:10.1193/1.2791001.
- [474] [35] S. Werner, C. Taylor, S. Cho, J. Lavoie, REDARS 2 methodology and software for seismic risk analysis of highway systems (technical manual), Tech. rep., Seismic Systems & Engineering Analysis for MCEER, Oakland, CA (2006).
- [475] [36] Caltrans, Caltrans Seismic Design Criteria Version 1.7, Tech. Rep. SDC 1.7, California Department of Transportation, Sacramento, CA (2013).
- [476] [37] Bechtel/HNTB Team, Design Criteria Volume I, Version 1.2, Tech. rep., San Francisco Bay Area Rapid Transit District, San Francisco Bay Area Rapid Transit District Earthquake Safety Program (2008).
- [477] [38] N. Kurtz, J. Song, P. Gardoni, Time-varying seismic reliability analysis of representative US west coast bridge transportation networks, in: G. Deodatis, B. R. Ellingwood, D. M. Frangopol (Eds.), *Safety, Reliability, Risk and Life-Cycle Performance of Structures and Infrastructures*, CRC Press, 2014, pp. 655–662.
- [478] [39] J. Ghosh, K. Rokneddin, J. E. Padgett, L. Dueas-Osorio, Seismic reliability assessment of aging highway bridge networks with field instrumentation data and correlated failures. I: Methodology, *Earthquake Spectra* 30 (2) (2013) 795–817. doi:10.1193/040512EQS155M.
- [479] [40] S. Pugh, Construction statistics, Tech. rep., California Department of Transportation Division of Engineering Services (2012).
- [480] [41] K. Kockelman, Travel Behavior as Function of Accessibility, Land Use Mixing, and Land Use Balance: Evidence from San Francisco Bay Area, *Transportation Research Record: Journal of the Transportation Research Board* 1607 (-1) (1997) 116–125. doi:10.3141/1607-16.
- [481] [42] P. Waddell, F. Nourzad, Incorporating nonmotorized mode and neighborhood accessibility in an integrated land use and transportation model system, *Transportation Research Record: Journal of the Transportation Research Board* 1805 (-1) (2002) 119–127. doi:10.3141/1805-14.
- [482] [43] C. F. Manski, *Structural analysis of discrete data with econometric applications*, MIT Press, 1981.
- [483] [44] K. A. Small, H. S. Rosen, Applied welfare economics with discrete choice models, *Econometrica* 49 (1) (1981) 105–130. doi:10.2307/1911129.
- [484] [45] D. Ory, Personal communication (2013).
- [485] [46] United States Department of Transportation, Revised departmental guidance: valuation of travel time in economic analysis, US Department of Transportation, Washington, DC.
- [486] [47] G. Erhardt, P. Brinckerhoff, D. Ory, A. Sarvepalli, J. Freedman, J. Hood, B. Stabler, MTC's Travel Model One: applications of an activity-based model in its first year, in: *Innovations in Travel Modeling 2012*, Tampa, Florida, 2012, p. 9.
- [487] [48] P. Waddell, UrbanSim: modeling urban development for land use, transportation, and environmental planning, *Journal of the American*

- 518 Planning Association 68 (3) (2002) 297–314. doi:10.1080/01944360208976274.
- 519 [49] W. Davidson, P. Vovsha, J. Freedman, R. Donnelly, CT-RAMP family of activity-based models, in: Proceedings of the 33rd Australasian
520 Transport Research Forum (ATRF), Canberra, Australia, 2010, p. 15.
- 521 [50] H. Wakabayashi, H. Kameda, Network performance of highway systems under earthquake effects: a case study of the 1989 Loma Prieta
522 earthquake, in: Proceedings US-Japan Workshop on Earthquake Disaster Prevention for Lifeline Systems, 1992, pp. 215–232.
- 523 [51] U.S. Bureau of the Census, United States Census 2010, Tech. rep., U.S. Census Bureau, Washington D.C. (2010).